Journal of ELECTRONIC MATERIALS, Vol. 45, No. 10, 2016
DOI: 10.1007/s11664-016-4675-2

Synthesis of $NiCo_2O_4$ Microellipsoids as Anode Material for Lithium-Ion Batteries

HAO ZHENG,[1,2] SHAN XU,[1] LIN LI,[2] CHUANQI FENG,[1] and SHIQUAN WANG[1,3]

1.—Hubei Collaborative Innovation Center for Advanced Organic Chemical Materials & the Ministry of Education Key Laboratory for Synthesis and Applications of Organic Functional Molecules, Hubei University, Wuhan 430062, China. 2.—Key Laboratory of Functional Materials and Chemistry for Performance and Resource of Guizhou Education Department, Anshun University, Anshun 561000, China. 3.—e-mail: wsqhao@126.com

$NiCo_2O_4$ microellipsoids have been synthesized by a rheological-phase hydrothermal method to obtain the precursors followed by annealing at 450°C for 4 h. The effects of different hydrothermal temperatures (140°C to 180°C) on the morphologies and electrochemical properties of the final product were systematically investigated. $NiCo_2O_4$ microellipsoids synthesized at 180°C exhibited the best electrochemical properties, with high reversible capacity (921 mAh g^{-1} at current density of 100 mA g^{-1}) and good cycling stability (820 mAh g^{-1} even after 100 cycles), compared with other samples. They also delivered discharge capacity of 586 mAh g^{-1} at relatively high current density of 800 mA g^{-1}. The remarkable electrochemical performance of the $NiCo_2O_4$ microellipsoids can be attributed to their high surface area. These results indicate that $NiCo_2O_4$ microellipsoids could be a promising electrode material for lithium-ion batteries.

Key words: Inorganic synthesis, electrochemical properties, energy storage, lithium-ion batteries

INTRODUCTION

Over the past few years, with the increase in portable electronics and electrical vehicles, the demand for rechargeable lithium-ion batteries (LIBs) has significantly increased.[1–3] It is essential to develop electrode materials with low cost, high energy density, good durability, and high safety.[4] Graphite, the anode material currently used in commercial LIBs, has relatively low capacity of 370 mAh g^{-1}. Thus, it is necessary to search for alternative anode materials for lithium-ion batteries with improved energy density and safety.[5] Transition-metal oxides (such as CoO_x,[6] FeO_x,[7] V_2O_5,[8] WO_3,[9] SnO_x,[10,11] etc.) have been demonstrated to have high reversible capacities at relatively low potential, being intensively investigated as possible substitutes for graphite anodes to meet higher requirements for electrochemical energy storage.

Employment of metal oxides in lithium-ion batteries is still largely hampered by poor long-term cycling stability and low electronic conductivity. One effective way to alleviate these problems is to fabricate nanostructured materials with high surface area, porous configuration, and short diffusion paths. Since Co_3O_4 exhibits inverse spinel structure and has been found to show good Li cyclability with high capacities, studies have been reported, as can be expected, on substituted Co_3O_4.[12] Various forms of Co_3O_4 have been reported to exhibit high and reversible capacities of 700 mAh g^{-1} to 950 mAh g^{-1}.[13–15] Comparative research on transition-metal oxides suggests that cobalt oxides have the best electrochemical properties as anodes, but the shortcomings of Co_3O_4 are that it is expensive and has high redox potential (2.2 V to 2.4 V versus Li^+/Li) for Co, restricting its broad application. MCo_2O_4 (M = Mg, Cu, Ni, Mn) compounds, with

(Received September 24, 2015; accepted May 13, 2016; published online June 3, 2016)

similar structure to Co_3O_4, are potential candidate anode materials for practical applications. Studies have been reported on compounds with the formula MCo_2O_4 (M = Ni, Mn, Fe, Cu, or Mg),[16–19] together with cycling profiles of selected compounds, including reversible capacity values and capacity retention by cycle number. Among metal oxides, cobalt-nickel oxide ($NiCo_2O_4$) is an interesting binary oxide semiconductor, being a very important transition-metal oxide with applications in lithium-ion batteries, due to its high theoretical specific capacity, low toxicity, and widespread availability. $NiCo_2O_4$, a well-known cobalt-nickel spinel oxide, features two solid-state redox couples (Co^{3+}/Co^{2+} and Ni^{3+}/Ni^{2+}) in its structure, enabling remarkable electrochemical activity.[20] Because of its better electrical conductivity and higher electrochemical activity compared with binary nickel oxide (NiO) or cobalt oxide (Co_3O_4), various $NiCo_2O_4$ morphologies, such as mesoporous structures,[19] nanoplates,[20] nanoparticles,[21] and nanowires,[22] have been prepared through various routes, including hydroxide decomposition, thermal treatment, hydrothermal synthesis, etc. Obviously, these advantages favor development of high-performance anode materials; For example, $NiCo_2O_4$ nanowires have been fabricated via a polymer/surfactant-assisted solution method, exhibiting high capacitance and good cycling stability.[23,24] The hydrothermal synthesis method is a promising approach for fabrication of low-dimensional hierarchically structured metal oxide thin films.[25] This method is facile, simple, and inexpensive, offers size control, requires low reaction temperatures, and is economic for large-scale production of materials with large surface area and unique morphology.[26] Lou and coworkers synthesized $NiCo_2O_4$ nanosheets/nanowires on conductive substrates that could achieve excellent cycling performance and rate capability.[27–29] More recently, Li et al. reported a simple template-free solvothermal route followed by thermal posttreatment of the precursor for synthesis of monodisperse $NiCo_2O_4$ mesoporous microspheres, which displayed superior battery performance. These $NiCo_2O_4$ microspheres exhibited high initial discharge capacity and could retain high capacity of 705 mAh g^{-1} at current density of 800 mA g^{-1}, even after 500 charge/discharge cycles.[19] Liu et al. reported a mild and cost-effective solution method to directly grow Ni-substituted Co_3O_4 (ternary $NiCo_2O_4$) nanorod arrays on Cu substrates. The $NiCo_2O_4$ nanorod arrays manifested high specific capacity, excellent cycling stability (with high reversible capacity of about 830 mAh g^{-1} achieved after 30 cycles at 0.5 C), and high rate capability.[22]

In this study, the precursor was synthesized via a rheological-phase hydrothermal method using $CoSO_4$, $NiSO_4$, and hexamethylenetetramine as reactants. $NiCo_2O_4$ microellipsoids were then fabricated through heat treatment at 450°C. The effects of different hydrothermal temperatures on the morphologies and electrochemical properties of the final product were investigated.

EXPERIMENTAL PROCEDURES

Synthesis and Characterization of Samples

All chemicals were of analytical grade and used without further purification. $NiSO_4{\cdot}2H_2O$, $CoSO_4{\cdot}2H_2O$, and hexamethylenetetramine were mechanically mixed at molar ratio of 1:2:6 in an agate mortar. After the mixture had been ground homogeneously, an appropriate amount of water was added to the powder to obtain a rheological-phase state mixture. After treating the above mixture at 140°C to 180°C for 24 h in a 50-mL Teflon-lined stainless-steel autoclave, it was cooled to room temperature. The precursors were collected, washed with deionized water and absolute ethanol, and dried in air at 80°C. The precursors were calcined at 450°C for 4 h under air atmosphere to obtain the final product (designated as $NiCo_2O_4$-140, $NiCo_2O_4$-160, and $NiCo_2O_4$-180, respectively).

Characterization

The structure and crystallinity of the samples were characterized using an x-ray diffractometer (XRD, Rigaku) with a Cu K_α radiation source (λ = 0.1506 nm) at voltage of 40 kV and current of 30 mA. Raman measurements were conducted at room temperature on a Jobin-Yvon HR800 Raman spectrometer attached to a charge-coupled device (CCD) camera, with an Ar^+ laser (514.4 nm) as excitation source. The morphologies of the samples were observed using scanning electron microscopy (SEM; LEO 1530VP, Germany) and transmission electron microscopy (TEM; Tecnai G2 F30, FEI Company).

Electrochemical Measurements

The electrochemical performance of the products was tested in a model test cell system. Positive electrodes were prepared by pressing a mixture of active material (70%), acetylene black (20%), and polytetrafluoroethylene (PTFE) (10%) onto a nickel grid. Prior to use, the positive electrodes were dried at 125°C in a vacuum furnace for 24 h. The electrolyte was a solution of 1 M $LiPF_6$ in ethylene carbonate (EC) and diethyl carbonate (DEC) (1:1 by volume). The separator was Celgard 2400 porous polypropylene. The counter and reference electrodes were lithium foil. The model test cells were assembled in an argon-filled glovebox. Charge/discharge tests were carried out at different current densities in the range from 0.01 V to 3.0 V. Cyclic voltammetry (CV) tests were carried out in the potential window of 0.01 V to 3.0 V on an electrochemical workstation (CHI 660). Electrochemical impedance spectroscopy (EIS) experiments were conducted in the frequency range of 0.01 kHz to 100 kHz on a CHI 600A electrochemical analyzer.

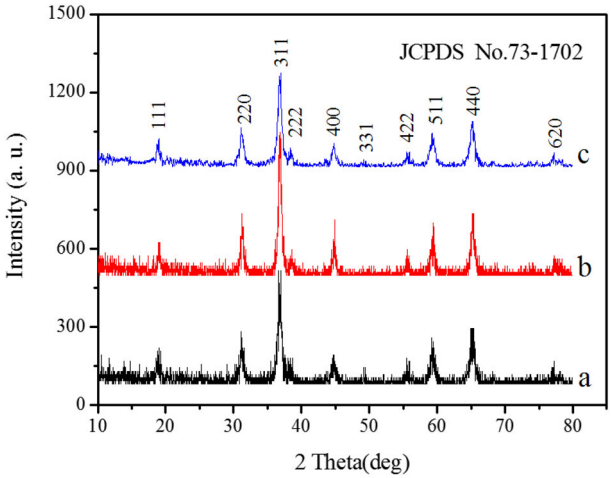

Fig. 1. XRD patterns of $NiCo_2O_4$ samples: (a) $NiCo_2O_4$-140, (b) $NiCo_2O_4$-160, and (c) $NiCo_2O_4$-180.

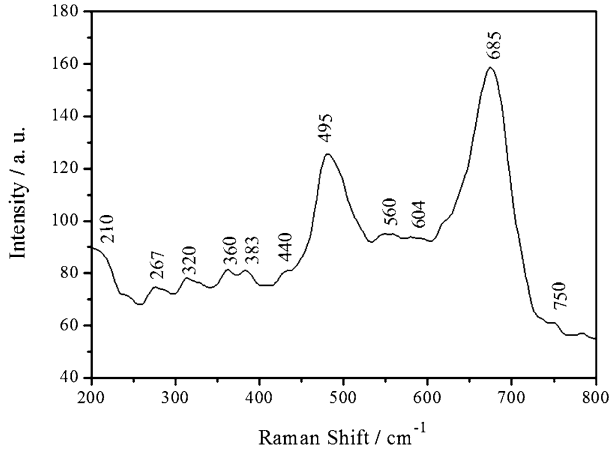

Fig. 2. Raman spectrum of $NiCo_2O_4$-180.

RESULTS AND DISCUSSION

Structure and Morphology Characterization

The XRD patterns of the as-prepared $NiCo_2O_4$ samples are presented in Fig. 1. Evidently, all the diffraction peaks can be readily assigned to the cubic spinel structure of $NiCo_2O_4$ [Joint Committee on Powder Diffraction Standards (JCPDS) card no. 73-1702] with lattice constant a = 8.269 Å. No other impurity peaks were observed in the XRD patterns, revealing that the three samples were pure spinel $NiCo_2O_4$. $NiCo_2O_4$-180 exhibited much narrow diffraction peaks than the other two samples ($NiCo_2O_4$-140 and $NiCo_2O_4$-160), indicating smaller crystallite size for this material. These results demonstrate that the simple thermal decomposition method is suitable for preparing multiple-transition-metal oxide nanomaterials, in which the molar ratios of transition-metal elements can be easily adjusted.[20–24]

Raman spectroscopy was used to provide vibrational information on the $NiCo_2O_4$-180 sample. A representative Raman spectrum of fresh $NiCo_2O_4$ electrode is shown in Fig. 2. The first two peaks located at 210 cm^{-1} and 360 cm^{-1} can be classified as a Ni–O lattice vibration mode.[30,31] The next two bands are one-phonon modes (TO at 400 cm^{-1} to 440 cm^{-1} and LO at 560 cm^{-1}), and a two-phonon mode (2TO at 750 cm^{-1}) of NiO.[32] Careful Raman spectroscopy of the Co–O lattice under appropriate measurement conditions, however, almost always revealed a typical, distinct feature, i.e., a strong Raman mode observed at 495 cm^{-1} and near 685 cm^{-1} region, with some Raman-active fundamentals (absorption at 685 cm^{-1}, 604 cm^{-1}, 440 cm^{-1}, 383 cm^{-1}, 320 cm^{-1}, 267 cm^{-1}, and 238 cm^{-1}) consistent with theoretical analysis.[33,34] This mode arises from the highest-frequency vibrational mode of CoO_6 octahedra, which is the symmetric stretching mode.

Figure 3 shows SEM images of the $NiCo_2O_4$ samples, demonstrating that they are spindle-like with diameter of around 6 μm to 15 μm. The $NiCo_2O_4$-140 sample was composed of nonuniform spindles 5 μm to 10 μm in length and particles of different sizes (Fig. 3a). The spindles become inhomogeneous due to agglomeration and decomposition of the spinel structure, and the grain size reaches several micrometers. With increasing hydrothermal temperature (160°C and 180°C), the as-obtained samples showed considerably larger spindles with more uniform size distribution (10 μm to 15 μm), as shown in Fig. 3b and c. The magnified image of a single spindle in Fig. 3d shows that the flakes self-assemble into spindles. The $NiCo_2O_4$-180 sample was mainly composed of nanoparticles, as can be seen in the low-magnification TEM image in Fig. 3e; the diameter of the nanoparticles could be estimated to be 20 nm to 50 nm. The high-magnification TEM image in Fig. 3f clearly presents a set of lattice fringes spaced at 0.245 nm, corresponding to (311) planes of $NiCo_2O_4$.[34]

Electrochemical Properties

Figure 4 shows the first five cyclic voltammetry (CV) curves of the electrode made from $NiCo_2O_4$-180 microellipsoids at scan rate of 0.1 mV/s. The voltammogram for the first cycle was substantially different from the subsequent ones. There was a strong cathodic peak at about 0.87 V versus Li/Li^+ during the first cycle of the CV scan, which can be ascribed to reduction of Ni^{2+} and Co^{3+} to metallic Ni and Co, respectively.[19,22] The main reduction peak shifts to lower potential of 0.85 V in subsequent cycles, which might originate from the pulverization of the $NiCo_2O_4$. The following anodic sweep was characterized by two oxidation peaks at ~1.6 V and ~2.2 V at the first cycle of the CV scan, which can be attributed to oxidation of Ni^0 to Ni^{2+} and Co^0 to Co^{3+}, and the peak shifts to higher potential of 2.28 V in the following cycles. Based on literature

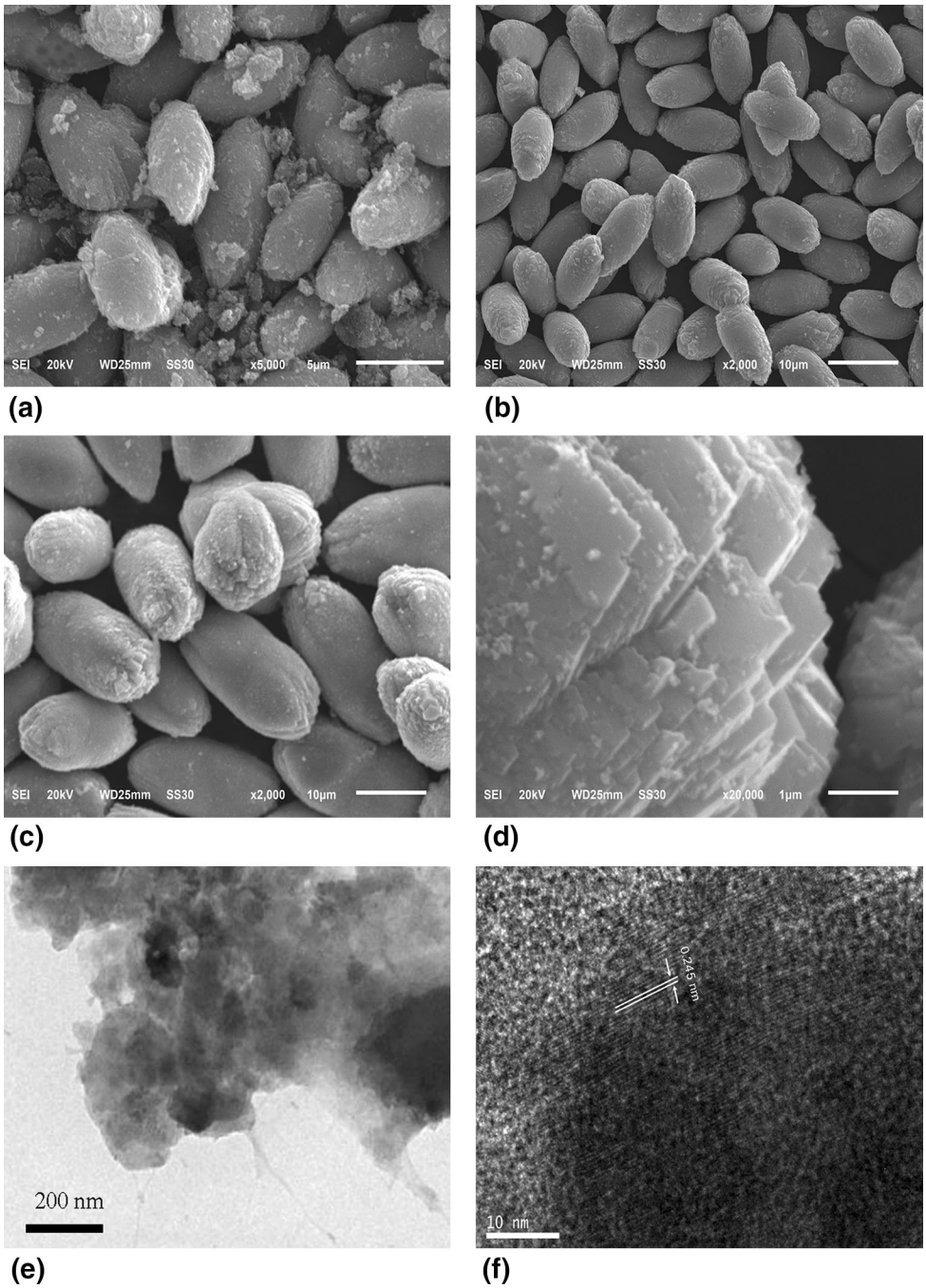

Fig. 3. SEM images of samples: (a) $NiCo_2O_4$-140, (b) $NiCo_2O_4$-160, and (c, d) $NiCo_2O_4$-180; TEM image (e) and high-resolution TEM image (f) of $NiCo_2O_4$-180.

and the cyclic voltammograms, the reversible insertion/extraction behavior of lithium should be amended as follows[19,22,29]:

$$NiCo_2O_4 + 8Li^+ + 8e^- \rightarrow Ni + 2Co + 4Li_2O \quad (1)$$

$$Ni + Li_2O \leftrightarrow NiO + 2Li^+ + 2e^- \quad (2)$$

$$Co + Li_2O \leftrightarrow CoO + 2Li^+ + 2e^- \quad (3)$$

$$CoO + 1/3Li_2O \leftrightarrow 1/3Co_3O_4 + 2/3Li^+ + 2/3e^- \quad (4)$$

When the $NiCo_2O_4$ microellipsoids are electrochemically discharged with lithium metal, destruction of the crystal structure occurs, followed by formation of Ni, Co, and Li_2O, as shown in Eq. 1. The consequent electrochemical process may be the combined reactions based on NiO and Co_3O_4, respectively. The electrochemical processes

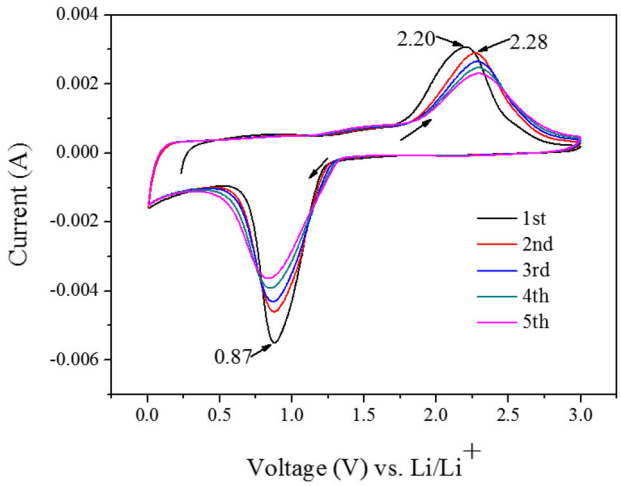

Fig. 4. First five CV cycles for $NiCo_2O_4$-180 microellipsoid electrode at scan rate of 0.1 mV s^{-1} in voltage range of 0.01 V to 3.0 V.

involving the individual NiO and Co_3O_4 components in the LIB anode have been clearly elucidated in many studies.[19]

The electrochemical performance of the $NiCo_2O_4$ microellipsoid samples was measured via coin cell testing. Figure 5 shows selected charge and discharge cycle profiles of the electrodes at current density of 100 mA g^{-1} in the range of 0.01 V to 3.0 V at room temperature. It can be seen that all these discharge curves exhibit one plateau between 0.8 V and 1.1 V. The initial discharge capacities of the as-prepared $NiCo_2O_4$-140, $NiCo_2O_4$-160, and $NiCo_2O_4$-180 samples were 1002 mAh g^{-1}, 1103 mAh g^{-1}, and 1121 mAh g^{-1} (equivalent to ~8.9 mol, 9.8 mol, and 10.0 mol Li per mole), respectively. Among them, the plateau of the first discharge curve was slightly lower than for the following curves, consistent with the CV results above.

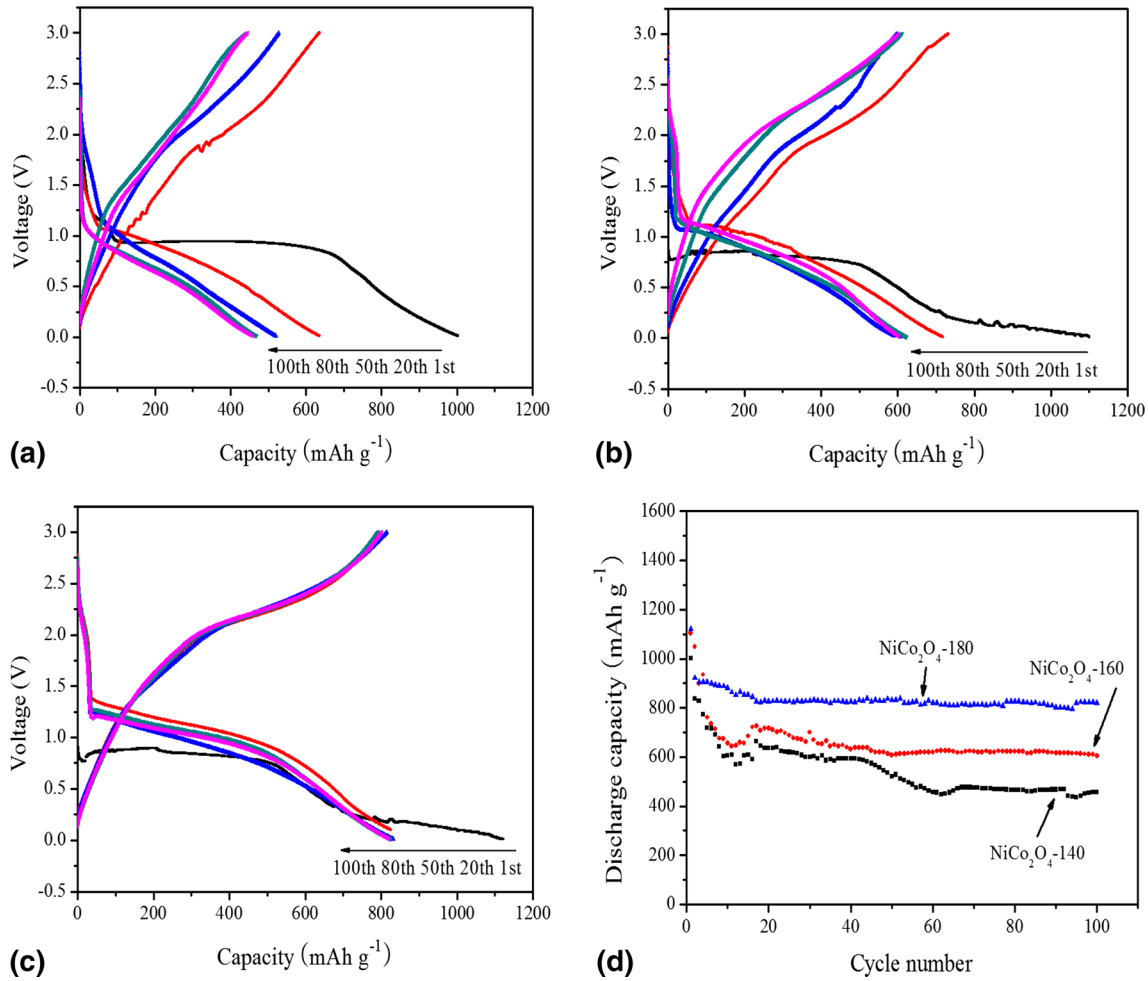

Fig. 5. Typical discharge/charge curves of (a) $NiCo_2O_4$-140, (b) $NiCo_2O_4$-160, and (c) $NiCo_2O_4$-180; (d) cycling performance of the three electrodes.

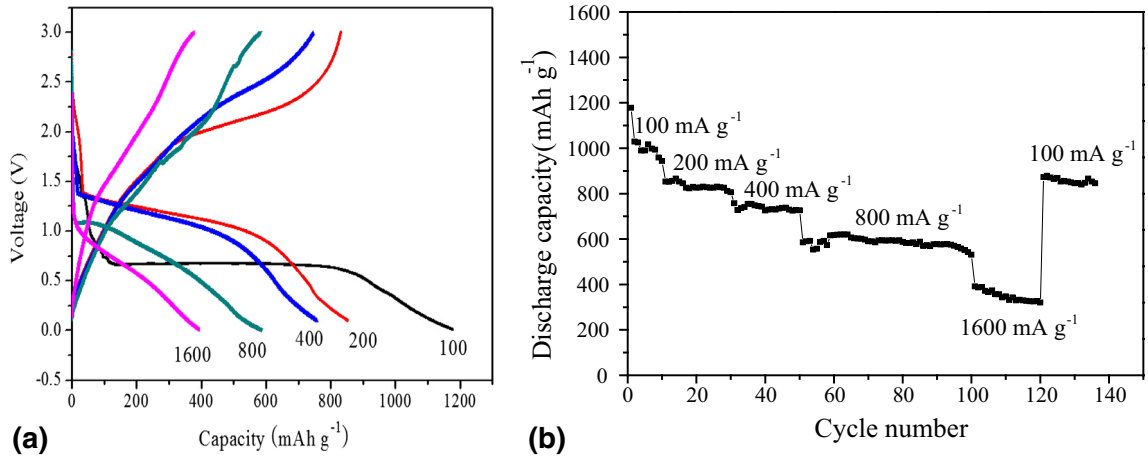

Fig. 6. (a) First discharge/charge cycle curves and (b) cycling performance of $NiCo_2O_4$-180 electrode at various current densities.

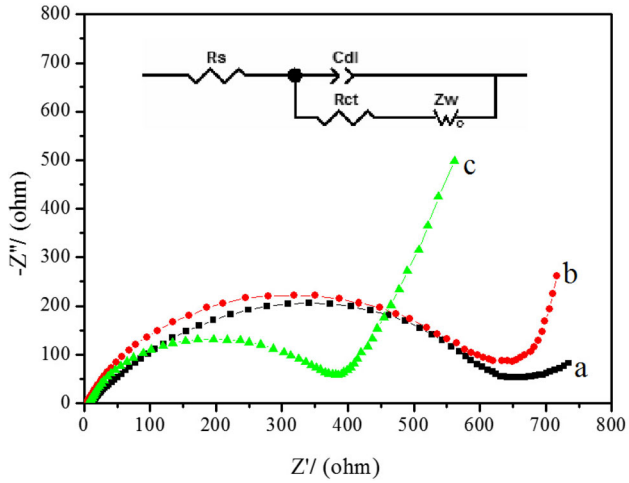

Fig. 7. Electrochemical impedance spectra (EIS) of (a) $NiCo_2O_4$-140, (b) $NiCo_2O_4$-160, and (c) $NiCo_2O_4$-180. Inset shows the equivalent circuit used to interpret the spectra.

The cycling performance of the samples at current density of 100 mA g^{-1} is shown in Fig. 5d. From these results, a large irreversible capacity at the first cycle was observed. The specific capacity of the $NiCo_2O_4$-140 and $NiCo_2O_4$-160 samples showed an obvious decrease with cycling, from 1002 mAh g^{-1} and 1102 mAh g^{-1} for the first cycle to 521 mAh g^{-1} and 607 mAh g^{-1} for the 50th cycle, respectively. The $NiCo_2O_4$-180 sample delivered a larger initial capacity of 1121 mAh g^{-1} (equivalent to ~11.4 mol Li per mole) and showed high reversible capacity of 921 mAh g^{-1} for the second cycle, much higher than reported for such samples.[19] Among them, the $NiCo_2O_4$-180 sample exhibited the best performance for Li^+ insertion. It still retained high capacity of 833 mAh g^{-1} after 50 cycles, and 820 mAh g^{-1} even after 100 cycles. It was obvious that the $NiCo_2O_4$-180 electrode showed greatly improved cycling performance with higher specific capacity at the same cycle number and current density, compared with the other samples, which may be attributed to its large surface area.

To better understand the electrochemical behavior of the spindle-shaped $NiCo_2O_4$ microellipsoids, we also investigated their rate performance, as shown in Fig. 6. The $NiCo_2O_4$-180 electrode was cycled at various current densities (100 mA g^{-1} to 1600 mA g^{-1}). The cell showed good rate capability with average discharge capacity of 1177 mAh g^{-1}, 852 mAh g^{-1}, 757 mAh g^{-1}, 586 mAh g^{-1}, and 391 mAh g^{-1} as the current density was increased stepwise to 100 mA g^{-1}, 200 mA g^{-1}, 400 mA g^{-1}, 800 mA g^{-1}, and 1600 mA g^{-1}, respectively. Upon returning the current density to 100 mA g^{-1}, average discharge capacity as high as 873 mAh g^{-1} could be recovered. This demonstrates that the $NiCo_2O_4$ microellipsoid structure has great potential as high-rate anode material in lithium-ion batteries, considering that high current density is very significant for practical batteries when fast discharge/charge is required. As shown in Fig. 6b, the discharge capacity decreased from the initial value of 586 mAh g^{-1} at relatively high current density of 800 mA g^{-1}. It slowly dropped to 530 mAh g^{-1} after 50 cycles, with Coulombic efficiency of around 90.4%. The microellipsoids offer the advantages of higher surface area and greater freedom for electrode volume change during charge/discharge processes.[19] The large surface area and short diffusion length in microellipsoid-structured electrodes could improve the kinetic properties of lithium ions during intercalation and easily deliver high discharge capacity, even under extremely high currents.

Electrochemical impedance spectroscopy (EIS) is a versatile electrochemical tool to characterize the intrinsic electrical properties of any material and its interfaces. Figure 7 presents the EIS spectra of the

$NiCo_2O_4$ samples, collected from fresh cells. The appearance of the high-frequency semicircle can be attributed to the formation of the solid electrolyte interphase film and/or contact resistance, while the medium-frequency region is assigned to the charge-transfer impedance on the electrode–electrolyte interface. It is clearly observed that the semicircle for the $NiCo_2O_4$-180 electrode (324 Ω) is smaller than for the other two samples (612 Ω and 571 Ω for $NiCo_2O_4$-140 and $NiCo_2O_4$-160, respectively), indicating that the $NiCo_2O_4$-180 electrode possesses lower contact and charge-transfer impedance. This confirms that the $NiCo_2O_4$-180 microellipsoids have better electrochemical properties, suitable for electrode material in lithium-ion batteries.

CONCLUSIONS

We have shown that $NiCo_2O_4$ electrodes can be synthesized via a rheological-phase hydrothermal method followed by annealing at 450°C for 4 h. When used as anode material for LIBs, the as-prepared $NiCo_2O_4$-180 showed the highest specific discharge capacity, superior rate capability, and excellent cycling stability compared with other samples. The $NiCo_2O_4$-180 electrode showed initial capacity of 1121 mAh g^{-1} at current density of 100 mA g^{-1}. After 100 cycles, it still retained high capacity of 820 mAh g^{-1}. Even when the current density was increased to 800 mA g^{-1}, the reversible capacity still reached 530 mAh g^{-1} after 50 cycles. This improved electrochemical performance makes such $NiCo_2O_4$ microellipsoids a promising anode material for next-generation, high-power lithium-ion batteries.

ACKNOWLEDGEMENTS

This work was financially supported by the Joint Science and Technology Funds of the Guizhou Science and Technology Department, Anshun City People's Government and Anshun University (Grant No. LKA [2013]17, LKA [2012]02), the Special and Key Laboratory of Functional Materials and Resource Chemistry of the Guizhou Provincial Education Department, Anshun University (GAFMRC201305).

REFERENCES

1. J.M. Tarascon and M. Armand, *Nature* 414, 359 (2001).
2. J.O. Besenhard and M. Winter, *Pure Appl. Chem.* 70, 603 (1998).
3. R. Wagner, N. Preschitschek, S. Passerini, J. Leker, and M. Winter, *J. Appl. Electrochem.* 43, 481 (2013).
4. T. Ohzuku and R. Brodd, *J. Power Sources* 174, 449 (2007).
5. M.V. Reddy, G.V. Subba Rao, and B.V.R. Chowdari, *Chem. Rev.* 113, 5364 (2013).
6. G.P. Kim, S.M. Park, I. Nam, J. Park, and J. Yi, *J. Mater. Chem. A* 1, 3872 (2013).
7. D.N. Lei, M. Zhang, B.H. Qu, L.B. Chen, Y.G. Wang, E.D. Zhang, Z. Xu, Q.H. Li, and T.H. Wang, *Nanoscale* 4, 3422 (2012).
8. A.Q. Pan, H.B. Wu, L. Zhang, and X.W. Lou, *Energy Environ. Sci.* 6, 1476 (2013).
9. W.J. Li and Z.W. Fu, *Appl. Surf. Sci.* 256, 2447 (2010).
10. J.S. Pen, T. Brousse, L. Sanchez, J. Morales, and D.M. Schleich, *J. Power Sources* 232, 97 (2001).
11. Z.G. Wen, F. Zheng, and K.L. Liu, *Mater. Lett.* 68, 469 (2012).
12. G.M. Zhou, L. Li, Q. Zhang, N. Lia, and F. Li, *Phys. Chem. Chem. Phys.* 15, 5582 (2013).
13. Z.S. Wu, W.C. Ren, L. Wen, L.B. Gao, J.P. Zhao, Z.P. Chen, G.M. Zhou, F. Li, and H.M. Cheng, *ACS Nano* 4, 3187 (2010).
14. L.J. Zhi, Y.S. Hu, B.E. Hamaoui, X. Wang, I. Lieberwirth, U. Kolb, J. Maier, and K. Mullen, *Adv. Mater.* 20, 1727 (2008).
15. S.B. Yang, X.L. Feng, S. Ivanovici, and K. Mullen, *Angew. Chem. Int. Ed.* 49, 8408 (2010).
16. R. Alcántara, M. Jaraba, P. Lavela, and J.L. Tirado, *Chem. Mater.* 14, 2847 (2002).
17. C.C. Ai, M.C. Yin, C.W. Wang, and J. Sun, *J. Mater. Sci.* 39, 1077 (2004).
18. Y. Sharma, N. Sharma, G.V.S. Rao, and B.V.R. Chowdari, *J. Power Sources* 173, 495 (2007).
19. J.F. Li, S.L. Xiong, Y.R. Liu, Z.C. Ju, and Y.T. Qian, *ACS Appl. Mater. Interfaces* 5, 981 (2013).
20. B. Cui, H. Lin, Y.Z. Liu, J.B. Li, P. Sun, X.C. Zhao, and C.J. Liu, *J. Phys. Chem. C* 113, 14083 (2009).
21. M. Srivastava, M.E. Uddin, J. Singh, N.H. Kim, and J.H. Lee, *J. Alloy. Compd.* 590, 266 (2014).
22. J. Liu, C.P. Liu, Y.L. Wan, W. Liu, Z.S. Ma, S.M. Ji, J.B. Wang, Y.C. Zhou, P. Hodgson, and Y.C. Li, *CrystEngComm* 15, 1578 (2013).
23. H.L. Wang, Q.M. Gao, and L. Jiang, *Small* 7, 2454 (2011).
24. H. Jiang, J. Ma, and C.Z. Li, *Chem. Commun.* 48, 4465 (2012).
25. P.N. Bhosale, V.V. Kondalkar, R.M. Mane, S. Choudhury, and K.V. Khot, *J. Nanomed. Nanotechnol.* 6, 103 (2015). doi:10.4172/2157-7439.1000e103.
26. L.F. Hu, L.M. Wu, M.Y. Liao, X.H. Hu, and X.S. Fang, *Adv. Funct. Mater.* 22, 998 (2012).
27. G.Q. Zhang, H.B. Wu, H.E. Hoster, M.B. Chan-Park, and X.W. Lou, *Energy Environ. Sci.* 5, 9453 (2012).
28. C.Z. Yuan, L. Yang, L. Hou, L.F. Shen, X.G. Zhang, and X.W. Lou, *Energy Environ. Sci.* 5, 7883 (2012).
29. S.L. Xiong, J.S. Chen, X.W. Lou, and H.C. Zeng, *Adv. Funct. Mater.* 22, 861 (2012).
30. H. Kishimotoa, K. Yashirob, T. Shimonosonoa, M.E. Britoa, K. Yamajia, T. Horitaa, H. Yokokawaa, and J. Mizusakib, *Electrochim. Acta* 8, 2263 (2012).
31. S. Deabate, F. Fourgeot, and F. Henn, *J. Power Sources* 87, 125 (2000).
32. B.S. Yeo and A.T. Bell, *J. Phys. Chem. C* 116, 8394 (2012).
33. H.M. Du, L.F. Jiao, Q.H. Wang, J.Q. Yang, L.J. Guo, Y.C. Si, Y.J. Wang, and H.T. Yuan, *Nano. Res.* 6, 87 (2013).
34. Y.C. Dong, M.J. Hu, R.G. Ma, H. Cheng, S.L. Yang, Y.Y. Li, and J.A. Zapien, *CrystEngComm* 15, 1324 (2013).